



First-principle prediction of structural and mechanical properties in NbMoTaWRe_x refractory high-entropy alloys with experimental validation

Jin-Yong Mo, Yi-Xing Wan, Zhi-Bin Zhang, Xin Wang, Xiao-Qing Li, Bao-Long Shen* , Xiu-Bing Liang* 

Received: 31 December 2021 / Revised: 12 February 2022 / Accepted: 20 February 2022 / Published online: 17 August 2022
© Youke Publishing Co., Ltd. 2022

In this work, the effect of Re alloying on the phase composition, crystal structure, and mechanical properties of NbMoTaWRe_x ($x = 0, 0.27, 0.57, 0.92, 1.33$) refractory high-entropy alloys (RHEAs) were systematically investigated by combining the calculation of phase diagram (CALPHAD), first-principle calculations and experiment. The theoretical predictions showed good consistency with the experimental results. As the increase in Re content, the theoretical results showed that all considered alloys have a single body-centered cubic (bcc) structure and the lattice constant and ductility were decreased, while the elastic moduli and hardness were improved. To avoid extreme brittleness, a strategic suggestion was given for the design of Re-containing RHEAs in the future.

Over the past decade, refractory high-entropy alloys (RHEAs) have drawn extensive attention due to their superior mechanical properties and potential application in the aerospace and nuclear industry. Composed of refractory

elements like Cr, Mo, Nb, V, Ta, W, Hf, Zr, Ti and Re, RHEAs show the ability to retain exceptional strength at elevated temperatures. In 2010, Senkov et al. [1, 2] proposed two representative RHEAs, NbMoTaW and NbMoTaWV, with impressive yield strength over 400 MPa at 1600 °C, far above the limits of ~ 900 °C for conventional Ni-based superalloys. Since then, many efforts have been devoted to further improving their performance. To explore high performance RHEAs, various elements have been added in NbMoTaW and NbMoTaWV, including metals such as Al [3], Cr [4], Ti [5–8], Zr [9] and non-metallic elements such as C [10, 11], Si [12, 13], B [14] and N [15, 16]. By employing the first-principle method, Tong et al. [17] and Liu et al. [18] investigated the effects of alloying on the structure, electronic and mechanical properties of NbMoTaWX, where X is Cr, V, Ti, Zr, Hf or Re, respectively.

Among the alloying elements mentioned above, Re is an effective solid solution strengthener in refractory alloys [19] and plays a crucial role in Ni-based superalloys [20–24]. It was reported that the fracture toughness of W-Re alloys increases with the increasing Re content [19]. Fleischmann et al. [25] compared the influence of the addition of Re, Mo and W in single-crystal Ni-based superalloy. All three elements can remarkably reduce the creep rate at elevated temperature, while Re is more than two times effective for the strengthening of alloy [25]. Considering the effect of Re in Ni-based superalloys, it is expected that Re can also serve as an effective strengthening element in RHEAs. However, the development of Re-containing RHEAs is relatively insufficient [26], and the mechanism of Re alloying is still far from clear. Some Re-containing RHEAs, including CrMoReVW [27], Mo₁₅Nb₂₀Re₁₅Ta₃₀W₂₀ [28], Mo₁₅Nb₂₀Re₁₅Ta₃₀W₂₀ [29],

J.-Y. Mo, Y.-X. Wan
School of Chemistry and Chemical Engineering, China
University of Mining and Technology, Xuzhou 221116, China

J.-Y. Mo, Z.-B. Zhang, X. Wang, X.-B. Liang*
Defense Innovation Institute, Academy of Military Science,
Beijing 100071, China
e-mail: liangxb_d@163.com

X.-Q. Li
Department of Materials Science and Engineering, KTH Royal
Institute of Technology, 10044 Stockholm, Sweden

B.-L. Shen*
School of Materials Science and Engineering, Jiangsu Key
Laboratory for Advanced Metallic Materials, Southeast
University, Nanjing 211189, China
e-mail: blshen@seu.edu.cn



Nb-Mo-Re-Ru-Rh [30], MoNbRe_{0.5}TaW [31] and ReMo-TaW, have been investigated theoretically or experimentally, but a systematic study of Re alloying effect on the properties of NbMoTaW is still lacking.

CALPHAD [32] and first-principle calculations [33] have been proven to be powerful tools in the designing of novel high-entropy alloys [34]. To further explore Re-containing RHEAs, we investigated the structure and mechanical properties of NbMoTaWRe_x ($x = 0, 0.27, 0.57, 0.92, 1.33$) RHEAs by combining the CALPHAD, first-principle calculation and experimental methods. First, the most possible equilibrium phases of NbMoTaWRe_x RHEAs were predicted by CALPHAD method. Then, the lattice constant, elastic modulus, hardness, and Pugh ratio of these RHEAs were calculated by the first-principle method. Furthermore, the as-cast alloys were prepared and the structure and mechanical properties were characterized experimentally, and the results were compared with the theoretical predictions.

The thermodynamic equilibrium phase diagrams of NbMoTaWRe_x ($x = 0, 0.27, 0.57, 0.92, 1.33$, hereafter denoted as NbMoTaW, Re0.27, Re0.57, Re0.92 and Re1.33, respectively) RHEAs were calculated using the Thermo-Calc software (version 2021a) and the TCHEA database (version 4.2) [32, 35].

Two widely used first-principle methods were applied in this work to predict the lattice constant, bulk modulus, shear modulus, Young's modulus, hardness, and Pugh ratio. The first method is the special quasi-random structure (SQS) method [36] combined with the projector augmented wave (PAW) method as implemented in the Vienna Ab initio Simulation Package (VASP) [37]. In this method, the disordered body-centered cubic (bcc) SQS structures with 128 atoms ($4 \times 4 \times 4$) were generated for each composition. The exchange–correlation functional is described by the generalized-gradient approximation (GGA) of Perdew-Burke-Ernzerhof (PBE) [38]. The plane-wave cutoff was set to 600 eV, with the convergence criteria of energy as 1×10^{-7} eV and criteria of force as $0.1 \text{ eV}\cdot\text{nm}^{-1}$. The Brillouin zone was sampled by the Monkhorst–Pack scheme with a k -point grid of $2 \times 2 \times 2$. The second method is the coherent potential approximation (CPA) [39, 40] combined with the Exact Muffin-Tin Orbital (EMTO) method [41, 42]. In this method, PBE [38] was chosen as the exchange–correlation functional and the screened impurity model parameter of CPA was set to 0.602 [43].

To study the elastic properties, the tetragonal shear modulus (C') and shear modulus (C_{44}) are obtained by using the orthorhombic deformation described as:

$$\begin{pmatrix} 1 + \varepsilon_0 & 0 & 0 \\ 0 & 1 - \varepsilon_0 & 0 \\ 0 & 0 & 1/(1 - \varepsilon_0^2) \end{pmatrix} \quad (1)$$

and monoclinic deformation:

$$\begin{pmatrix} 1 & \varepsilon_m & 0 \\ \varepsilon_m & 1 & 0 \\ 0 & 0 & 1/(1 - \varepsilon_m^2) \end{pmatrix} \quad (2)$$

The strain ε_0 and ε_m are from 0 to 0.025 with step of 0.005. By further combining $C' = (C_{11} - C_{12})/2$ and bulk modulus (B) = $(C_{11} + 2C_{12})/3$, we obtained the value of C_{11} and C_{12} . Finally, the polycrystalline shear modulus (G) was obtained as $G = (G_V + G_R)/2$, where $G_V = (C_{11} - C_{12} + 3C_{44})/5$ and $G_R = 5(C_{11} - C_{12})C_{44}/(3C_{11} - 3C_{12} + 4C_{44})$. The Young's modulus (E) is derived as $E = 9BG/(3B + G)$, and hardness (H_V) is derived as $H_V = 2(k^2G)^{0.585} - 3$, where $k = G/B$ [44]. To convert GPa to HV, the value of hardness is further divided by 0.009807.

To predict the equilibrium phases in the investigated alloys, phase diagrams are calculated using Thermo-calc software with TCHEA (v5.0) database. Figure 1a shows the predicted phase equilibria in the isopleth for the series of NbMoTaWRe_x, where $x = 0-1.5$ represents the moles of atoms of the element Re. According to Fig. 1a, the liquidus temperature of the investigated alloys does not change much with the increase in Re element. Cooling from the liquids, the alloys first form a disordered bcc solid solutions structure (bcc #1) and then a second bcc phase (bcc #2) with concentrated W element precipitated from the matrix phase at ~ 1000 K. Figure 1b, c displays the predicted relative mole fraction of phase as a function of temperature for NbMoTaW and Re1.33 HEAs, respectively. As shown in Fig. 1b, the NbMoTaW HEA in solid-state forms a single bcc phase at all temperatures, which agrees well with the experimental results [1]. The liquidus temperature (T_{liq}) and solidus temperature (T_{sol}) of NbMoTaW are 3136 and 3077 K, respectively. The predicted T_{liq} of NbMoTaW is close to the value (3177 K) estimated by rule-of-mixture (ROM) method [45]. For Re1.33 alloy, the calculated T_{liq} , T_{sol} and decomposition temperature (T_{dec}) are 3222, 3060 and 1737 K, respectively (Fig. 1c).

It is important to note that the RHEAs obtained via arc-melting are usually not thermodynamic equilibrium owing to the fast cooling rate and thus the actually observed phase structure of the as-cast alloys will not follow the prediction of CALPHAD [46]. The cooling rate of arc-melting is $\sim 1 \text{ K}\cdot\text{s}^{-1}$. In such condition, there is not enough time to

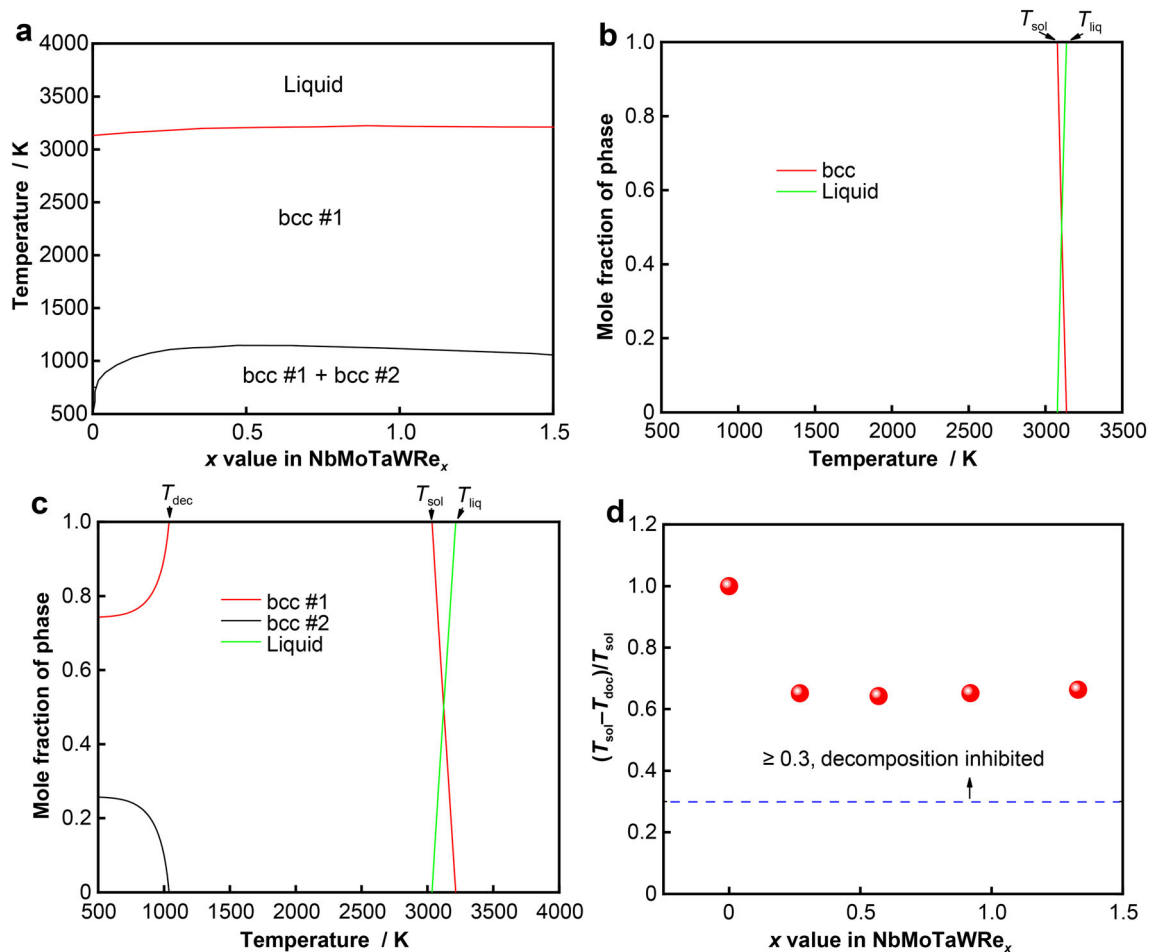


Fig. 1 **a** Equilibrium phase diagram of NbMoTaWRe_x ($x = 0, 0.27, 0.57, 0.92, 1.33$) RHEAs; **b** phase diagram of NbMoTaW and **c** Re1.33; **d** ratios of $(T_{sol} - T_{dec})/T_{sol}$ of NbMoTaWRe_x ($x = 0, 0.27, 0.57, 0.92, 1.33$) RHEAs

Table 1 Nominal compositions of NbMoTaWRe_x ($x = 0, 0.27, 0.57, 0.92, 1.33$) RHEAs and calculated δ , ΔH_{mix} and ΔS_{mix} of each composition

Alloys	Composition / at%					δ	ΔH_{mix} / (kJ·mol ⁻¹)	ΔS_{mix} / (J·K ⁻¹ ·mol ⁻¹)
	Nb	Mo	Ta	W	Hf			
NbMoTaW	25	25	25	25	–	2.31	– 6.50	11.52
Re0.27	23.4375	23.4375	23.4375	23.4375	6.25	2.27	– 9.29	12.75
Re0.57	21.8750	21.8750	21.8750	21.8750	12.50	2.23	– 11.65	13.22
Re0.92	20.3125	20.3125	20.3125	20.3125	18.75	2.18	– 13.58	13.38
Re1.33	18.7500	18.7500	18.7500	18.7500	25	2.12	– 15.09	13.32

achieve equilibrium state. To predict the non-equilibrium phases, some empirical criteria are proposed. For example, it is believed that the phase decomposition at low temperature may be inhibited in as-cast RHEAs when the ratio $(T_{sol} - T_{dec})/T_{sol}$ is larger than 0.30 [47]. As shown in Fig. 1d, the ratio of $(T_{sol} - T_{dec})/T_{sol}$ for NbMoTaW is 1, because there is no decomposition in this composition. With Re addition, the ratio gradually decreased to 0.43 in

Re1.33. Because all the NbMoTaWRe_x HEAs considered in this work have a larger ratio of $(T_{sol} - T_{dec})/T_{sol}$ than the critical ratio of 0.30, it is very likely that the decomposition at low temperature will be inhibited. Actually, it has been proven in many studies that the phase decomposition will be inhibited in many as-cast refractory alloys [46–48]. The atomic radius difference (δ), enthalpy of mixing (ΔH_{mix}) and entropy of mixing (ΔS_{mix}) were also calculated to



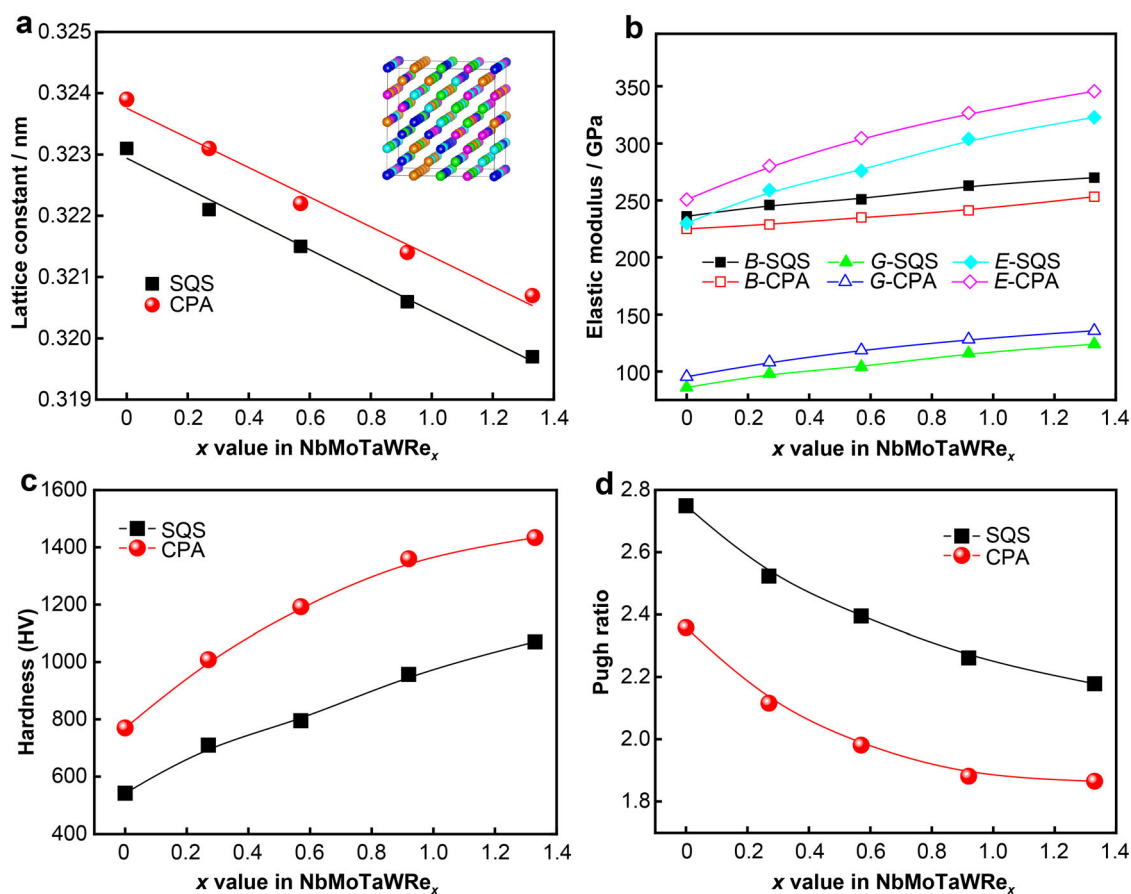


Fig. 2 Calculated **a** lattice constant; **b** elastic modulus including *B*, *G* and *E*; **c** hardness; and **d** Pugh ratio of NbMoTaWRe_x RHEAs

further estimate the phases, which are shown in Table 1. The calculated δ , ΔH_{mix} and ΔS_{mix} are in the range of 2.12%–2.31%, -15.09 to -6.50 kJ·mol⁻¹ and 11.52–13.32 J·K⁻¹·mol⁻¹, respectively. The results meet the criterion, suggested by Guo and Liu [49] as $0 \leq \delta \leq 8.5$, $-22 \leq \Delta H_{\text{mix}} \leq 7$ kJ·mol⁻¹ and $11 \leq \Delta S_{\text{mix}} \leq 19.5$ J·K⁻¹·mol⁻¹, for the formation of solid-solution phase in HEAs. Based on the above results, the as-cast NbMoTaWRe_x RHEAs are expected to have a single bcc solid-solution structure.

After determining the most likely crystal structure of NbMoTaWRe_x RHEAs, we predict their lattice constant and mechanical properties, such as elastic modulus, hardness, and Pugh ratios by density functional theory (DFT) calculations. Figure 2a shows the lattice constants of bcc NbMoTaWRe_x RHEAs calculated by both EMT0 and VASP methods, and the inset figure illustrates the SQS model of NbMoTaW employed in the VASP calculations. Our results show that it has a steady decline in lattice constant with the increase in Re content. It also can be found that the lattice constants predicted by EMT0 are slightly larger than the values predicted by VASP, with a difference in value of ~ 0.001 nm ($\sim 0.3\%$).

Figure 2b shows the theoretical elastic modulus, including bulk modulus (*B*), Young's modulus (*E*) and shear modulus (*G*) of NbMoTaWRe_x RHEAs from the SQS and CPA methods. The corresponding values can be found in Table 2. With the content of Re increasing, all the three moduli show an increasing trend. The predicted trends in the elastic moduli from SQS and CPA show good consistency, and the difference in values is less than 8%. For NbMoTaW, the values of *B*, *G* and *E* calculated using SQS are 236 GPa (225 GPa in CPA calculation), 86 GPa (95 GPa in CPA calculation), and 230 GPa (251 GPa in CPA calculation), respectively. The predicted elastic moduli of NbMoTaW agree well with the results reported by Tong et al. [17]. With the Re content *x* increasing from 0 to 1.33, the SQS predicted an increase of bulk modulus from 236 to 270 GPa (from 225 to 253 GPa in the CPA method), Young's modulus increases from 230 to 331 GPa (from 251 to 358 GPa in the CPA method), and shear modulus increases from 86 to 124 GPa (from 95 to 136 GPa in the CPA method). The hardness of NbMoTaWRe_x RHEAs is also gradually improved with the increasing of Re content, as shown in Fig. 2c. With the Re content *x* increasing from 0 to 1.33, the hardness increases from HV 542 to HV 1071

in SQS prediction and from HV 770 to HV 1434 in CPA calculations, respectively. The difference in hardness from the two methods is larger than that of elastic modulus. This is because the hardness is estimated from the elastic modulus. Despite the numerical difference, the calculations from CPA and SQS show a very similar trend with the addition of Re.

B/G ratio is often used to study the ductile–brittle behavior of materials [50–52]. According to the Pugh criterion, a material with a B/G ratio larger than 1.75 often behaves in a ductile manner, while material with Pugh ratio smaller than 1.75 shows a brittle behavior [53]. However, Frantsevich et al. suggested B/G ratio of ~ 2.67 as the critical value to distinguish the ductile/brittle materials [54, 55]. To estimate the ductile–brittle behavior of NbMoTaWRe_x RHEAs, the Pugh ratio was calculated by both CPA and SQS methods, as shown in Fig. 2d. In this work, B/G ratio of NbMoTaW obtained from SQS and CPA are 2.749 and 2.358, respectively. Meanwhile, Liu et al. reported B/G ratio of NbMoTaW predicted by the SQS method as 2.587 and 2.565, respectively [17, 18]. These results, from both SQS and CPA, are much higher than the Pugh's criterion 1.75. However, according to the report of Senkov et al. [2], NbMoTaW has a plastic strain about 2.0%. These theoretical results may suggest that the Pugh's criterion 1.75 is not large enough to estimate the ductile–brittle behavior of NbMoTaW-based RHEAs. With the increase in Re content, B/G ratio obtained by the SQS method decreased from 2.749 to 2.178, while the ratio obtained by the CPA method decreased from 2.358 to

1.865. The reduced B/G ratio implies an increased intrinsic brittleness as the Re content increases. Considering the limited ductility of NbMoTaW, it is reasonable to expect a more brittle behavior in NbMoTaWRe_x RHEAs.

To verify the DFT results, the NbMoTaWRe_x RHEAs were prepared by vacuum arc-melting method and the crystal structure and mechanical properties were characterized. Figure 3a displays XRD patterns of the as-cast NbMoTaWRe_x RHEAs. All XRD peaks are identified with appropriate indices, and it proves that all NbMoTaWRe_x RHEAs have single bcc structures, which agrees with the prediction of CALPHAD and empirical parameter calculations. As shown in Fig. 3b, the lattice constant is linearly decreased with the increasing of Re, which is consistent with the trend obtained from SQS and CPA methods. Furthermore, the measured data are very close to the theoretical values (Table 2).

The room-temperature engineering compressive stress–strain curves of NbMoTaWRe_x RHEAs are shown in Fig. 4a. The measured yield strength, maximum strength, and plastic strain of NbMoTaW are 1163 MPa, 1269 MPa and 2.01%, respectively. It can be seen clearly that the plastic strain is decreased with the addition of Re. The inset in Fig. 4a shows that the slopes of the curves during the elastic deformation stage increase with the increasing Re content, suggesting that the Young's modulus, as the DFT calculations predicted, is improved after Re alloying. Moreover, after Re alloying, a series of sudden drops in stress can be seen at the elastic deformation stage. The sudden drops are the results of the brittle bursts of the

Table 2 Lattice constant (a), B , G and E , hardness and Pugh ratio of NbMoTaWRe_x RHEAs from present theory

Alloys	Methods	a / nm	B / GPa	G / GPa	E / GPa	Hardness (HV)	B/G
NbMoTaW	SQS	0.3231	236	86	230	542	2.749
	SQS [56]	–	236	92	245	–	2.565
	CPA	0.3239	225	95	251	770	2.358
	Exp	0.3230	–	–	72	543 ± 13	–
Re0.27	SQS	0.3221	246	98	259	710	2.523
	CPA	0.3231	229	108	280	1008	2.116
	Exp	0.3219	–	–	86	575 ± 16	–
Re0.57	SQS	0.3215	251	104	276	795	2.395
	CPA	0.3222	235	119	305	1192	1.981
	Exp	0.3210	–	–	91	603 ± 11	–
Re0.92	SQS	0.3206	263	116	304	957	2.261
	CPA	0.3214	241	128	327	1360	1.881
	Exp	0.3200	–	–	93	607 ± 10	–
Re1.33	SQS	0.3197	270	124	323	1071	2.178
	CPA	0.3207	253	136	346	1434	1.865
	Exp	0.3195	–	–	114	634 ± 21	–

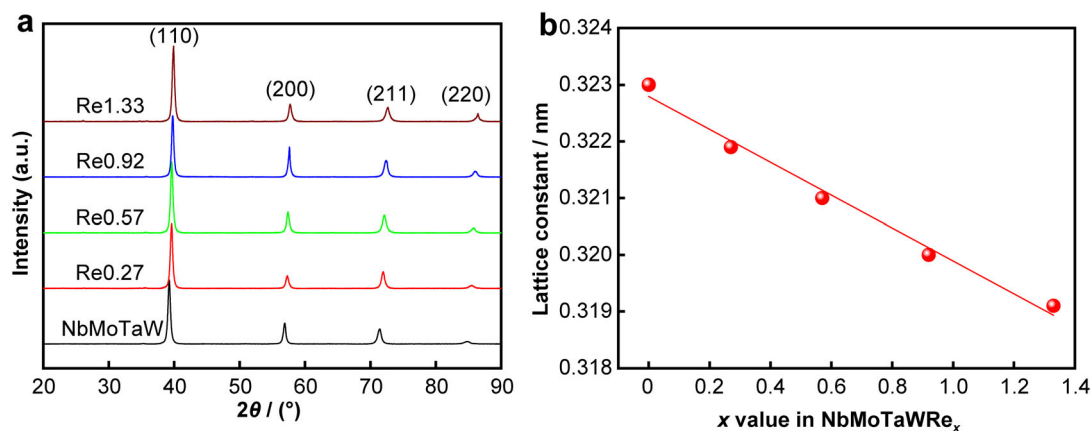


Fig. 3 a XRD patterns and b lattice constants of NbMoTaWRe_x HEAs from experiments

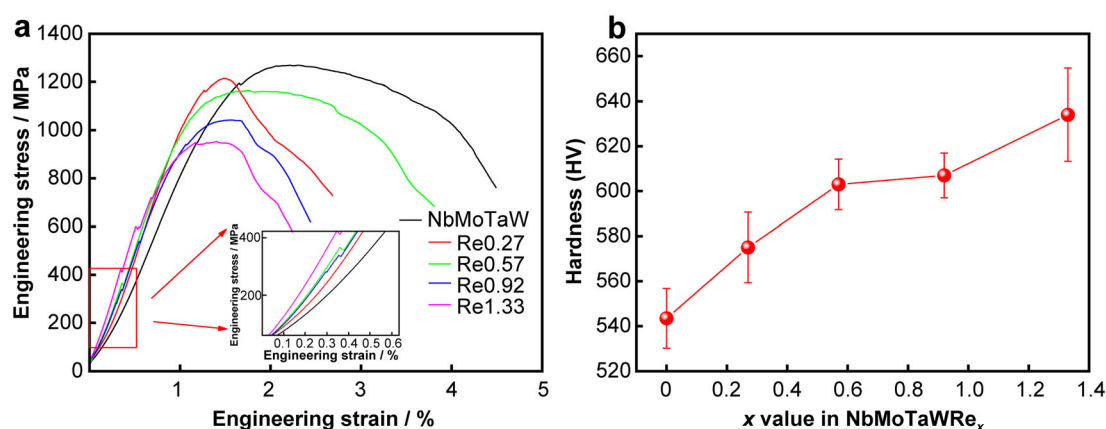


Fig. 4 a Room-temperature engineering compressive stress–strain and (inset) enlarged image in strain range of 0–0.6%, and b hardness of NbMoTaWRe_x RHEAs from experiments

samples under compression. Meanwhile, the sudden drops are more obvious in alloys with high Re contents (Re0.92 and Re1.33). These results suggest that the alloys become very brittle after Re alloying, which is consistent with the theoretical prediction. In fact, the content of Re in Ni-based superalloys is usually not larger than 3 wt% because of the rareness of Re and the Re-induced brittleness [20, 21]. In Re0.57 RHEAs, the content of Re is 8.23 wt% (6.25 at%), which is much higher than the limit of 3 wt%. Considering the very limited ductility of NbMoTaW, the traditional design idea that each component has a concentration of about 5 at%–35 at% is not suggested when alloying with Re. In order to maintain reasonable levels of ductility, it is necessary to limit the content of Re in NbMoTaW or simultaneously alloying Re with other elements that can improve the ductility, such as Zr [17].

Figure 4b shows the dependence of the Vickers hardness on the content of Re. As shown in this figure, the hardness is gradually increased with the increase in Re content. The

hardness of NbMoTaW is HV (543 ± 13), and in Re1.33 the hardness increases to HV (634 ± 21). The trend of the hardness with the addition of Re is consistent with the prediction of SQS and CPA calculations (Fig. 2c).

In summary, the effect of Re alloying on the phase composition, crystal structure, and mechanical properties of NbMoTaWRe_x ($x = 0, 0.27, 0.57, 0.92, 1.33$) RHEAs was investigated by combining the CALPHAD, first-principle calculations, and experimental methods. All considered RHEAs were predicted to have single bcc structure from CALPHAD and empirical criteria, which was verified by XRD characterizations. As the increase in Re content, the hardness was gradually improved from HV (543 ± 16) (NbMoTaW) to HV (634 ± 21) (Re1.33), and the Young's modulus was also gradually increased. However, the addition of Re leads to an increase in brittleness. Overall, the predictions from DFT methods are consistent with the experimental results quantitatively (such as lattice constants) or qualitatively (such as elastic moduli, hardness,

and brittleness). In order to avoid extreme brittleness, we suggest that the alloying of Re should be added in a lower concentration or alloying Re with other ductile elements simultaneously.

Acknowledgements This work was financially supported by the National Key R&D Program of China (No. 2018YFC1902400), the National Natural Science Foundation of China (No. 51975582), and the Program of China Scholarship Council (No. 202006420036).

Declarations

Conflict of interests The authors declare that they have no conflict of interest.

References

- [1] Senkov ON, Wilks GB, Miracle DB, Chuang CP, Liaw PK. Refractory high-entropy alloys. *Intermetallics*. 2010;18(9):1758.
- [2] Senkov ON, Wilks GB, Scott JM, Miracle DB. Mechanical properties of $Nb_{25}Mo_{25}Ta_{25}W_{25}$ and $V_{20}Nb_{20}Mo_{20}Ta_{20}W_{20}$ refractory high entropy alloys. *Intermetallics*. 2011;19(5):698.
- [3] Bachani SK, Wang CJ, Lou BS, Chang LC, Lee JW. Microstructural characterization, mechanical property and corrosion behavior of VNbMoTaWAl refractory high entropy alloy coatings: effect of Al content. *Surf Coat Technol*. 2020;403:126351.
- [4] Long Y, Liang X, Su K, Peng H, Li X. A fine-grained NbMoTaWVCr refractory high-entropy alloy with ultra-high strength: microstructural evolution and mechanical properties. *J Alloys Compd*. 2019;780:607.
- [5] Han ZD, Chen N, Zhao SF, Fan LW, Yang GN, Shao Y, Yao KF. Effect of Ti additions on mechanical properties of NbMoTaW and VNbMoTaW refractory high entropy alloys. *Intermetallics*. 2017;84:153.
- [6] Han ZD, Luan HW, Liu X, Chen N, Li XY, Shao Y, Yao KF. Microstructures and mechanical properties of Ti NbMoTaW refractory high-entropy alloys. *Mater Sci Eng A*. 2018;712:380.
- [7] Kalali DG, Antharam S, Hasan M, Karthik PS, Phani PS, Rao KBS, Rajulapati KV. On the origins of ultra-high hardness and strain gradient plasticity in multi-phase nanocrystalline MoNbTaTiW based refractory high-entropy alloy. *Mater Sci Eng A*. 2021;812:141098.
- [8] Xiao B, Jia W, Tang H, Wang J, Zhou L. Microstructure and mechanical properties of WMoTaNbTi refractory high-entropy alloys fabricated by selective electron beam melting. *J mater sci technol*. 2022;108:54.
- [9] Li T, Jiao W, Miao J, Lu Y, Guo E, Wang T, Li T, Liaw PK. A novel ZrNbMoTaW refractory high-entropy alloy with in-situ forming heterogeneous structure. *Mater Sci Eng A*. 2021;827:142061.
- [10] Wan Y, Wang X, Zhang Z, Mo J, Shen B, Liang X. Structures and properties of the $(NbMoTaW)_{100-x}C_x$ high-entropy composites. *J Alloys Compd*. 2021;889:161645.
- [11] Luo G, Jiang S, Wei Q, Kang K, Qian Y, Zhang J, Sun Y, Shen Q. Microstructure and mechanical properties of $MoNbW(TaC)_x$ composites. *Int J Refract Met Hard Mater*. 2021;99:105574.
- [12] Guo Z, Zhang A, Han J, Meng J. Effect of Si additions on microstructure and mechanical properties of refractory NbTaWMo high-entropy alloys. *J Mater Sci*. 2019;54(7):5844.
- [13] Ge Y, Cheng J, Yan C, Zhang B, Zhu S, Xue L, Hong S, Wu Y, Zhang Z, Liang X. Thermally induced microstructure evolution and effects on the corrosion behaviors of AlFeSi metallic glass coatings. *Intermetallics*. 2022;143:107473.
- [14] Hung SB, Wang CJ, Chen YY, Lee JW, Li CL. Thermal and corrosion properties of V-Nb-Mo-Ta-W and V-Nb-Mo-Ta-W-Cr-B high entropy alloy coatings. *Surf Coat Technol*. 2019;375:802.
- [15] Li H, Jiang N, Li J, Huang J, Kong J, Xiong D. Hard and tough $(NbTaMoW)N_x$ high entropy nitride films with sub-stoichiometric nitrogen. *J Alloys Compd*. 2021;889:161713.
- [16] Xia A, Dedoncker R, Glushko O, Cordill MJ, Depla D, Franz R. Influence of the nitrogen content on the structure and properties of MoNbTaVW high entropy alloy thin films. *J Alloys Compd*. 2021;850:156740.
- [17] Tong Y, Bai L, Liang X, Chen Y, Zhang Z, Liu J, Li Y, Hu Y. Influence of alloying elements on mechanical and electronic properties of NbMoTaWX (X = Cr, Zr, V, Hf and Re) refractory high entropy alloys. *Intermetallics*. 2020;126:106928.
- [18] Liu H, Liu L, Xin C. Effect of alloying elements on the structure and mechanical properties of NbMoTaWX (X = Cr, V, Ti, Zr, and Hf) refractory high-entropy alloys. *AIP Adv*. 2021;11(2):025044.
- [19] Mutoh Y, Ichikawa K, Nagata K, Takeuchi M. Effect of rhenium addition on fracture toughness of tungsten at elevated temperatures. *J Mater Sci*. 1995;30(3):770.
- [20] Rae CMF, Reed RC. The precipitation of topologically close-packed phases in rhenium-containing superalloys. *Acta Mater*. 2001;49(19):4113.
- [21] Fink PJ, Miller JL, Konitzer DG. Rhenium reduction alloy design using an economically strategic element. *JOM*. 2010;62(1):55.
- [22] Kurzynowski T, Smolina I, Kobiela K, Kuźnicka B, Chlebus E. Wear and corrosion behaviour of Inconel 718 laser surface alloyed with rhenium. *Mater Des*. 2017;132:349.
- [23] Heckl A, Neumeier S, Göken M, Singer RF. The effect of Re and Ru on γ/γ' microstructure, γ -solid solution strengthening and creep strength in nickel-base superalloys. *Mater Sci Eng A*. 2011;528(9):3435.
- [24] Fleischmann E, Konrad C, Preußner J, Völkl R, Affeldt E, Glatzel U. Influence of solid solution hardening on creep properties of single-crystal nickel-based superalloys. *Metall Mater Trans A*. 2015;46(3):1125.
- [25] Fleischmann E, Miller MK, Affeldt E, Glatzel U. Quantitative experimental determination of the solid solution hardening potential of rhenium, tungsten and molybdenum in single-crystal nickel-based superalloys. *Acta Mater*. 2015;87:350.
- [26] Senkov ON, Miracle DB, Chaput KJ, Couzinie JP. Development and exploration of refractory high entropy alloys—a review. *J Mater Res*. 2018;33(19):3092.
- [27] Raturi A, Aditya CJ, Gurao NP, Biswas K. ICME approach to explore equiatomic and non-equiatomic single phase BCC refractory high entropy alloys. *J Alloys Compd*. 2019;806:587.
- [28] Zhang C, Bhandari U, Zeng C, Ding H, Guo S, Yan J, Yang S. Carbide formation in refractory $Mo_{15}Nb_{20}Re_{15}Ta_{30}W_{20}$ alloy under a combined high-pressure and high-temperature condition. *Entropy (Basel)*. 2020;22(7):718.
- [29] Bhandari U, Zhang C, Zeng C, Guo S, Yang S. Computational and experimental investigation of refractory high entropy alloy $Mo_{15}Nb_{20}Re_{15}Ta_{30}W_{20}$. *J Mater Res Technol*. 2020;9(4):8929.
- [30] Liu B, Wu J, Cui Y, Zhu Q, Xiao G, Wu S, Cao GH, Ren Z. Structural evolution and superconductivity tuned by valence electron concentration in the Nb-Mo-Re-Ru-Rh high-entropy alloys. *J mater sci technol*. 2021;85:11.
- [31] Wei Q, Luo G, Zhang J, Chen P, Shen Q, Zhang L. Effect of raw material forms on the microstructure and mechanical properties of MoNbRe_{0.5}TaW high-entropy alloy. *Mater Sci Eng A*. 2020;794:139632.



- [32] Mao H, Chen HL, Chen Q. TCHEA1: a thermodynamic database not limited for “high entropy” alloys. *J Ph Equilibria Diffus*. 2017;38(4):353.
- [33] Xiong K, Wang BW, Sun ZP, Li W, Jin CC, Zhang SM, Xu SY, Guo L, Mao Y. First-principles prediction of elastic, electronic, and thermodynamic properties of high entropy carbide ceramic (TiZrNbTa)C. *Rare Met*. 2022;41(3):1002.
- [34] Yang HX, Li JS, Guo T, Wang WY, Kou HC, Wang J. Evolution of microstructure and hardness in a dual-phase Al_{0.5}CoCr-FeNi high-entropy alloy with different grain sizes. *Rare Met*. 2020;39(2):156.
- [35] Chen HL, Mao H, Chen Q. Database development and Calphad calculations for high entropy alloys: challenges, strategies, and tips. *Mater Chem Phys*. 2018;210:279.
- [36] van de Walle A, Tiwary P, de Jong M, Olmsted DL, Asta M, Dick A, Shin D, Wang Y, Chen LQ, Liu ZK. Efficient stochastic generation of special quasirandom structures. *Calphad*. 2013;42:13.
- [37] Kresse F. Efficient iterative schemes for ab initio total-energy calculations using a plane-wave basis set. *Phys Rev B*. 1996;54(16):11169.
- [38] Blochl PE. Projector augmented-wave method. *Phys Rev B Condens Matter*. 1994;50(24):17953.
- [39] Soven P. Coherent-potential model of substitutional disordered alloys. *Phys Rev*. 1967;156(3):809.
- [40] Gyorfyy BL. Coherent-potential approximation for a nonoverlapping-muffin-tin-potential model of random substitutional alloys. *Phys Rev B*. 1972;5(6):2382.
- [41] Vitos L. Total-energy method based on the exact muffin-tin orbitals theory. *Phys Rev B*. 2001;64(1):014107.
- [42] Vitos L. *Computational Quantum Mechanics for Materials Engineers: the EMTO Method and Applications*, Edited. Berlin: Springer Science and Business Media; 2007.86.
- [43] Korzhavyi P, Ruban A, Abrikosov I, Skriver HL. Madelung energy for random metallic alloys in the coherent potential approximation. *Phys Rev B*. 1995;51(9):5773.
- [44] Chen XQ, Niu H, Li D, Li Y. Modeling hardness of polycrystalline materials and bulk metallic glasses. *Intermetallics*. 2011;19(9):1275.
- [45] Liu Y, Zhang YA, Wang W, Li DS, Ma YJ. Influence of rare earth Y on microstructure and high temperature oxidation behavior of Ni-Fe-Co-Cu alloy. *Chin J Rare Met*. 2020;44(1):9.
- [46] Wang SP, Ma E, Xu J. New ternary equi-atomic refractory medium-entropy alloys with tensile ductility: hafnium versus titanium into NbTa-based solution. *Intermetallics*. 2019;107:15.
- [47] Yao HW, Qiao JW, Hawk JA, Zhou HF, Chen MW, Gao MC. Mechanical properties of refractory high-entropy alloys: experiments and modeling. *J Alloys Compd*. 2017;696:1139.
- [48] An Z, Mao S, Liu Y, Wang L, Zhou H, Gan B, Zhang Z, Han X. A novel HfNbTaTiV high-entropy alloy of superior mechanical properties designed on the principle of maximum lattice distortion. *J mater sci technol*. 2021;79:109.
- [49] Guo S, Liu CT. Phase stability in high entropy alloys: formation of solid-solution phase or amorphous phase. *Prog Nat Sci*. 2011;21(6):433.
- [50] Ge H, Tian F, Wang Y. Elastic and thermal properties of refractory high-entropy alloys from first-principles calculations. *Comput Mater Sci*. 2017;128:185.
- [51] Zhang H, Sun X, Lu S, Dong Z, Ding X, Wang Y, Vitos L. Elastic properties of Al_xCrMnFeCoNi (0 ≤ x ≤ 5) high-entropy alloys from ab initio theory. *Acta Mater*. 2018;155:12.
- [52] Huang S, Li W, Eriksson O, Vitos L. Chemical ordering controlled thermo-elasticity of AlTiVCr_{1-x}Nb high-entropy alloys. *Acta Mater*. 2020;199:53.
- [53] Pugh SF. XCII. Relations between the elastic moduli and the plastic properties of polycrystalline pure metals. *Lond Edinb Dublin Philos Mag J Sci*. 1954;45(367):823.
- [54] Frantsevich IN, Voronov FF, Bokuta SA. *Elastic Constants and Elastic Moduli of Metals and Insulators Handbook*. 1983. 107.
- [55] Cui S, Feng W, Hu H, Feng Z, Liu H. Hexagonal Ti₂SC with high hardness and brittleness: a first-principles study. *Scripta Mater*. 2009;61(6):576.
- [56] Hu YL, Bai LH, Tong YG, Deng DY, Liang XB, Zhang J, Li YJ, Chen YX. First-principle calculation investigation of NbMo-TaW based refractory high entropy alloys. *J Alloys Compd*. 2020;827:153963.